Author Accepted Manuscript version of the paper by Robert Johnson et al.
in ACS Sustainable Chemistry & Engineering Vol. 11 (2023) Page, DOI: http://dx.doi.org/10.1021/acssuschemeng.2c05229

Use of Plasticized Biochar Intermediate for Producing Biocarbons with Improved Mechanical Properties

Journal:	*ACS Sustainable Chemistry & Engineering*
Manuscript ID	sc-2022-05229m.R4
Manuscript Type:	Article
Date Submitted by the Author:	n/a
Complete List of Authors:	Johnson, Robert; University of Hawai'i at Manoa Castillo, Kyle; University of Hawai'i at Manoa Castillo, Christian; University of Hawai'i at Manoa Wang, Liang; SINTEF Energi AS, Thermal Energy Skreiberg, Øyvind; SINTEF Energi AS, Turn, Scott; University of Hawaii System, Hawaii Natural Energy Institute

Author Accepted Manuscript version of the paper by Robert Johnson et al.
in ACS Sustainable Chemistry & Engineering Vol. 11 (2023) Page, DOI: http://dx.doi.org/10.1021/acssuschemeng.2c05229

Use of Plasticized Biochar Intermediate for Producing Biocarbons with Improved Mechanical Properties

Robert L. Johnson[1*], Kyle Castillo[1], Christian Castillo[1], Liang Wang[2], Øyvind Skreiberg[2], Scott Q Turn[1]

[1] Hawaii Natural Energy Institute, University of Hawaii at Mānoa, 1680 East-West Rd., POST 109, Honolulu, Hawaii, 96822, USA

[2] SINTEF Energy Research, Sem Saelands vei 11, Trondheim, Norway

*Corresponding author email: robertlj@hawaii.edu

Abstract:

Slow pyrolysis of woody materials under elevated pressure was previously shown to result in macroscopic morphology changes, appearing as a solid that had experienced a molten phase, described as “transient plastic phase biochar” (TPPB). Experiments have been conducted to study the influence of process variables on the formation of TPPB. Results suggest TPPB formation is mediated through hydrolysis that allow for a molten phase to occur. Elevated pressure plays a key role by keeping water in the condensed phase. Despite drastic changes in material morphology, notable differences between TPPB and standard biochar (not TPPB or “NTPPB”) were not detected using proximate analysis, solid state ^{13}C NMR, and helium pycnometry, indicating the material chemistry was minimally affected. Clear differences between the mechanical properties of the TPPB and NTPPB powders and pellets were shown using tabletability experiments. The utility of TPPB was then demonstrated by comparison of tensile and compression strengths of materials calcined (N_2) at (900 ^oC) to form transient plastic phase biocarbon (TPPC). The TPPB precursor resulted in a TPPC pellet with 10 times greater tensile (4.4 MPa) and compressive strength (17.6 MPa) and nearly two times greater density than carbon pellets produced from NTPPB.

Author Accepted Manuscript version of the paper by Robert Johnson et al.
in ACS Sustainable Chemistry & Engineering Vol. 11 (2023) Page, DOI: http://dx.doi.org/10.1021/acssuschemeng.2c05229

Key Words: Transient-plastic-phase, Pressurized-pyrolysis, Decarbonization, Biocoke, Carbonization, Plasticity, Elasticity, Pellet strength

Author Accepted Manuscript version of the paper by Robert Johnson et al.
in ACS Sustainable Chemistry & Engineering Vol. 11 (2023) Page, DOI: http://dx.doi.org/10.1021/acssuschemeng.2c05229

Introduction:

An approach for reducing greenhouse gas emissions is thermochemical conversion of woody biomass into engineered carbon materials to displace those currently produced from fossil resources. The largest volumes of industrial carbon materials produced include coal tar pitch, carbon black, graphite, and calcined coke, which are used in electrode materials (aluminum manufacturing), metallurgic reductants (e.g. Mn), carbon binders, battery anodes, filler for tires, and ink components. [1] Applications for engineered carbon materials such as electrodes for the metallurgic industry and anodes for lithium-ion batteries, generally require high fixed carbon content (>90%), high crystallinity, low surface area, high compressive strength (40-50 MPa), high true density (>2.05 g/cc), low ash content and low coefficients of thermal expansion. Each application may have additional textural and physical specifications that require specialized processing and add to the cost of these products. Developing processes to produce engineered carbon materials from biomass presents a significant value proposition.

When considering the synthesis of carbon materials several key distinctions provide a basic framework for how different feedstocks will affect final properties, and the underlying processes which lead to the chemical structural development. The first key distinction is between graphitizable and non-graphitizable carbons, also referred to as soft and hard carbon, [2] and generally corresponds to the degree to which the material transforms via coking or charring. [3] Graphitizable carbon precursors carbonize via coking which involves formation of a molten phase that facilitates long range graphitic order to develop. Non-graphitizable precursors carbonize via charring and do not undergo a molten phase as strong bonds are formed that sterically prevent long range graphitic crystalline formation. Non-graphitizing materials which do undergo a molten phase such as poly-(furfural alcohol) result in glassy carbons. [3] The resulting material comprises tightly packed curved aromatic fragments that are extensively cross-linked, contain minimal porosity, and result in exceptional mechanical strength with compressive strength ranging from 200-800 MPa [2].

Author Accepted Manuscript version of the paper by Robert Johnson et al.
in ACS Sustainable Chemistry & Engineering Vol. 11 (2023) Page, DOI: http://dx.doi.org/10.1021/acssuschemeng.2c05229

Engineering material properties from a graphitizable substrate such as petroleum are relatively straightforward using thermal processing to modulate the extent of graphitization. Unlike petroleum, biomass is non-graphitizable and carbonizes exclusively via charring even when treated at temperatures in excess of 2000 °C. The high oxygen content and reactivity of biomass functional groups result in extensive crosslinking that occurs at relatively low temperatures compared to a glass transition temperature. The lack of a molten phase during biomass carbonization prevents tunability in the textural, electrical, and mechanical properties.[3] The conversion of biomass to fossil fuels by geochemical processes occurred because favorable temperature and pressure conditions, shear forces, and hydrothermal reactions sufficiently broke down the macro-molecular structure to allow the formation of high grade coal and graphite. [4, 5] Therefore, engineering biocarbon properties from biomass requires physical and/or chemical processes to prevent the extensive cross-linking characteristic of charring.

One approach is to use fast pyrolysis to convert the solid biomass into a bio-oil which can be further fractionated and used as a green-binder and/or as carbonization feedstock. [6-11] This processing route has been shown to significantly improve material properties, but requires multiple unit operations to thermochemically fractionate biomass components, reformulate to obtain desired mixtures, and finally carbonize to obtain the final product. The compressive strength reported for anodes produced from calcined petroleum cokes with bio-oil/pitch binders range from 22 to 36 MPa at binder content of 15 to 25 wt%. [6, 12] An alternative, pressurized thermochemical processing, avoids the bio-oil intermediate. One approach applies a compressive load (2-5 MPa) during heating (similar to ablative pyrolysis), resulting in a plasticized biochar that, with additional thermal processing, produces a carbonized material with higher density, improved graphitic order and reduced thermal expansion coefficient. [13] A pressurized hydrothermal or a gaseous reaction environment also alters the morphology of the biochar product by promoting secondary thermochemical reactions which are minimized or absent under standard pressure conditions.

Hydrothermal carbonization of biomass feedstocks has been extensively investigated over the last 20 years as a thermochemical route to engineered carbon materials for specific applications. [4] Low temperature (<300 °C)

Author Accepted Manuscript version of the paper by Robert Johnson et al.
in ACS Sustainable Chemistry & Engineering Vol. 11 (2023) Page, DOI: http://dx.doi.org/10.1021/acssuschemeng.2c05229

hydrothermal carbonization of carbohydrates and/or biomass leads to drastic changes in the material morphology, often resulting in uniform spherical structures. Like standard pyrolysis, hydrothermal conditions do not lead to greater development of extensive aromatic sheets, typical of charcoal formed at temperature >400 °C. [14-16] Direct formation of graphitic material requires hydrothermal conditions at temperatures in excess of 500 °C and under pressures approaching 100 MPa. [4] Scale up of a process that requires such extreme conditions presents significant technical obstacles. A hybrid approach, first producing a low temperature hydrochar as feedstock for a second high-temperature standard pyrolysis step resulted in improved graphitic order evident from high resolution transmission electron microscopy (HRTEM). [17] This hybrid approach was demonstrated with lignin (300 °C) with added metal catalysts in the second step to produce highly graphitic carbon materials at 900 °C. [18]

Pyrolysis with elevated pressure and/or constant volume conditions improve fixed carbon yields, and reduce reaction times. [19, 20] These effects were postulated to result from secondary char formation promoted by the increased residence time of volatile products within reactive proximity to the pyrolyzed solid material surfaces (including pores). The resulting bulk material would then comprise primary and secondary char products. Interestingly, solid biochar products recovered from a limited number of constant volume carbonization tests, appeared to have experienced a molten phase. These materials, labeled transient plastic phase biochars (TPPB) [19, 21, 22], were produced from microcrystalline cellulose, oak wood, and birch at temperatures as low as 300 °C. A systematic characterization of TPPB material properties was not reported nor were reaction conditions requisite for TPP formation. It is plausible that TPPB results from secondary char accumulation on the outer surfaces of the particles, leading to the appearance of a molten phase. This composite material would be a mixture of primary char derived from the parent biomass, coated by secondary char condensed from released volatiles. The prospect of using static pressure to plasticize and facilitate a molten phase could have significant implications as a tool for engineering biocarbon properties. Understanding the properties of TPPB and under what conditions it can be produced is an important fundamental question. Results from a well-designed series of experiments should be

Author Accepted Manuscript version of the paper by Robert Johnson et al.
in ACS Sustainable Chemistry & Engineering Vol. 11 (2023) Page, DOI: http://dx.doi.org/10.1021/acssuschemeng.2c05229

able to unambiguously determine if TPPB results from a molten phase, or secondary charcoal formation, or some combination of the two.

The analytical tools to quantify material properties of biochar powders including plasticity, thermal expansion, and elasticity would provide information related to macromolecular properties not easily accessed via other techniques. This analytical tool set would enable studies to determine how different reaction conditions, can be tuned for engineering biomass into biocarbon with improved mechanical properties. General morphology can be probed with scanning electron microscopy (SEM) and polarized light microscopy to obtain qualitative information. A quantitative measure to gauge how changes in morphology translate into mechanical properties would be extremely valuable. Solid state ^{13}C NMR is one spectroscopic technique sensitive to molecular dynamics of solids. Advanced experiments can be carried out using chemical shift anisotropy, dipolar couplings, and relaxation but require high level expertise to both acquire and interpret data and are therefore not easily accessible. Raman spectroscopy and X-ray diffraction (XRD) are excellent techniques for materials treated at high temperatures. Raman analysis compares peak areas for the D vs G bands corresponding to disordered and graphitic domains. [23] XRD can provide information on average crystallite sizes and compare levels of graphitic character between different materials. [24-26] Unfortunately, Raman and XRD data from low temperature biochar provides little useful information. Therefore, a straightforward analytical tool box to quantify macromolecular structure would be very useful for improving the mechanical properties of biocarbon materials.

Elasticity, plasticity, fracture strength, and ductility of powders compressed into tablets has been studied extensively using a universal tester, die, micrometer, balance, and helium pycnometer. [27-29] As a powder is compressed into a pellet, individual particles fracture and deform reducing the pore space between and within particles. Solid fraction (the ratio of apparent density to true density (eqn 1)) and porosity (eqn 2) of pellets can provide insight into differences between materials. If sufficient compressive force was applied to remove all void space, the apparent density would equal the true density. A solid fraction >1 is realized if the compressive load is great enough to compress the solid material itself. After the compressive load is released the pellet may expand

Author Accepted Manuscript version of the paper by Robert Johnson et al.
in ACS Sustainable Chemistry & Engineering Vol. 11 (2023) Page, DOI: http://dx.doi.org/10.1021/acssuschemeng.2c05229

in volume, the extent to which the material expands reflects the material elasticity. The extent to which a powdered material will form a stable pellet is directly related to the extent to which the material undergoes plastic deformation under a compressive load. Materials that deform elastically do not form stable pellets.

$$Solid\ Fraction = \frac{Apparent\ Density}{(True\ Density)} \quad (1)$$

$$Porosity = 1 - Solid\ Fraction \quad (2)$$

Van der Waals and London dispersion forces between particle surfaces are responsible for intra-pellet cohesion, and decrease rapidly with distance (inverse of distance to the sixth power). [29] The overall total strength of a pellet is the product of bonding strength and bonding area. Pellet strength increases when the powder undergoes fracture and plastic deformation by developing more bonding area, or contact surfaces between particles, within the pellet. Once formed the overall pellet strength can be determined by breaking the pellet. Diametric compression (force applied on the pellet diameter) is used to break the pellet and the measured maximum force (F_{max}) is used to calculate the tensile strength using (eqn 3). The compressive strength is determined by loading the pellet on the cylindrical axis and is calculated from the measured maximum force (F_{max}) using (eqn 4).

$$Tensile\ Strength = \frac{2Fmax}{(\pi * D * H)} \quad (3)$$

$$Compressive\ Strength = Fmax/(\pi r^2) \quad (4)$$

Where *D* is the pellet diameter, *H* is the pellet height (axial length), and *r* is the pellet radius.

Several important relationships can be used to compare pellets from different materials. [27-29]

- The compressibility profile (solid fraction vs compression pressure) reflects the degree to which particles fracture and undergo plastic deformation.
- The compactability profile (tensile strength vs solid fraction) reflects the relative strength holding individual particles together.

Author Accepted Manuscript version of the paper by Robert Johnson et al.
in ACS Sustainable Chemistry & Engineering Vol. 11 (2023) Page, DOI: http://dx.doi.org/10.1021/acssuschemeng.2c05229

- The tabletability profile (tensile strength vs compression pressure) reflects the overall suitability of the material to form pellets.
- The tensile modulus provides a measure of pellet ductility.

This paper reports results of experiments conducted to accomplish the following objectives.

1. Investigate the role of pressure and temperature as it pertains to TPPB formation.

2. Provide evidence to support or refute a molten phase explanation for TPPB formation, and develop a working model for TPPB formation.

3. Compare TPPB and NTPPB macro scale properties related to plasticity and elasticity through powder compression studies.

4. Demonstrate the utility of TPPB using secondary thermal processing to make enriched carbon materials and compare their mechanical strength to the TPPB and NTPPB precursors.

Materials and Methods:

Sample Preparation

Norwegian birch stem wood chips were ground into <2 mm and <4 mm size fractions using a rotary knife mill (Fritsch Pulverisette 19, Idar-Oberstein, Germany), and size fractionated using a sieve shaker (Rotap RX-29, WS Tyler, Mentor, OH) for 5 minute intervals. Material moisture content was determined by drying overnight at 105 ^{o}C or until constant weight. To produce test samples with moisture content greater than the equilibrium value of the parent birch (~10% wet basis), the prescribed amount of water and parent birch were added to an empty reactor, sealed, and allowed to equilibrate overnight (or longer as required). A fine powder sample was prepared by further grinding a 1-2 mm size fraction in a Retsch ZM 200 Ultra Centrifugal Mill to pass a 0.2 mm screen.

Biomass Pyrolysis

Author Accepted Manuscript version of the paper by Robert Johnson et al.
in ACS Sustainable Chemistry & Engineering Vol. 11 (2023) Page, DOI: http://dx.doi.org/10.1021/acssuschemeng.2c05229

General reactor design and procedure

All pressurized pyrolysis tests were run using the wall heated tube bomb (WHTB) reactor system described previously. [22] The reactor was updated to include a back pressure regulator (Swagelok 316 SS KPB series (0-20.7 MPa) with PEEK seats and 0.06 C_v) to allow for both constant volume and constant pressure reaction conditions (Scheme S1). An aluminum shroud was added to cover the top of the reactor to minimize heat and alundum loss from the sand bath. The following experiments utilized (1) a "double" reactor comprising two 25 mm paired WHTBs, (2) a "small" 12.5 mm single WHTB, and (3) a 12.5 mm, "partitioned" WHTB that used a screen to separate the reactor volume into two sub-volumes. The latter was used to verify whether biomass feedstock had experienced a molten phase.

After loading with biomass, the reactors were weighed, leak checked, purged, and pressurized using industrial nitrogen from a compressed gas cylinder. For each test, reactors were immersed in a temperature controlled sand bath for 30 min, with the starting time defined by the reactor making contact with the hot sand bath surface.

The system pressure for constant pressure pyrolysis was initially set using a N_2 compressed gas cylinder to 10-20% above the desired pressure with the back pressure regulator adjusted to 20.7 MPa. With the discharge from the BPR connected to a dry gas meter the BPR setpoint was reduced until flow was observed at the dry gas meter. The dry gas meter was then removed from the system and the pressure adjusted to the setpoint using the BPR.

When the test was completed the reactors were cooled to room temperature, depressurized, and weighed, and their contents quantitatively recovered.

Constant pressure WHTB reactions

Prior observance of TPPB was from constant volume WHTB tests. [19, 21, 22] Constant pressure WHTB tests were carried out to determine the role of pressure on the formation of TPPB. All constant pressure reactor tests were pressurized to the prescribed set point prior to being immersed in the sand bath. Gas was released through the

Author Accepted Manuscript version of the paper by Robert Johnson et al.
in ACS Sustainable Chemistry & Engineering Vol. 11 (2023) Page, DOI: http://dx.doi.org/10.1021/acssuschemeng.2c05229

back pressure valve as the system heated after immersion. This transient heating period produced a ~15% overshoot above the set point pressure while the system came to steady state.

A summary of constant pressure tests (CP Series) to determine the effect of pressure on TPPB formation is shown in Table 1. Tests with reactor pressures of 0, 0.69, 4.5 and 6.9 MPa were conducted at a temperature of 320 °C. These tests used the double reactor system with a three-point internal thermocouple. An average of the three temperatures is reported. All reactors were fully loaded with 1-2 mm birch particles (~28 g total) to replicate solid feedstock conditions across the test series.

Two additional tests were conducted to compare the effect of feedstock particle size. The fine powder material (< 0.2 mm) tests shown as IDs 10 and 11 in Table 1 were conducted as 0.69 and 12.4 MPa constant-pressure counter parts to IDs 2, 5, and 6.

The Melt Test series in Table 1 used the sectioned WHTB with the upper section of the reactor loaded with ~2.5 g of birch wood (2-4 mm) and the bottom section empty. The volume of the upper section was 70% of the total and the remaining 30% below the 1 mm screen. Under constant pressure (12.4 MPa) test conditions, generated gases would flow upwards out of the reactor and through the back pressure regulator. The material found in the bottom section of the reactor, would have passed through the 1 mm screen separating the two reactor sections, indicating that a molten phase had occurred. This test also verified that TPPB formation was not inhibited by a large void volume in the reactor.

Additional experiments were conducted to augment the constant pressure series and better understand the effect of temperature on TPPB formation. To this end, Tests 4 and 8 in Table 1 were conducted at the same constant pressure condition but at 320 and 420 °C, respectively.

An additional experiment was conducted to seek a lower temperature boundary for TPPB formation using a pressure that formed TPPB at 320°C and 30 minutes reaction time. Test 9 was conducted at 275 °C based on the results obtained from Test 6.

Author Accepted Manuscript version of the paper by Robert Johnson et al.
in ACS Sustainable Chemistry & Engineering Vol. 11 (2023) Page, DOI: http://dx.doi.org/10.1021/acssuschemeng.2c05229

206

Author Accepted Manuscript version of the paper by Robert Johnson et al.
in ACS Sustainable Chemistry & Engineering Vol. 11 (2023) Page, DOI: http://dx.doi.org/10.1021/acssuschemeng.2c05229

Table 1: Experiment list for constant pressure reactions. All reaction times were 30 minutes.

ID	Experiment	Biomass	Temp. °C	Reactor	Pressure (MPa)	Particle Size (mm)	H_2O wt %
1	CP Series	Birch	320	25 mm	0	1-2	8
2	CP Series	Birch	320	25 mm	0.69	1-2	8
3	CP Series	Birch	320	25 mm	4.5	1-2	8
4	CP Series	Birch	320	25 mm	6.9	1-2	8
5	CP Series	Birch	320	25 mm	10.3	1-2	8
6	Melt test	Birch	320	12.5 mm 2-section	12.4	2-4	20
7	Melt test (-) Control	Birch	320	12.5 mm 2-section	0.69	2-4	20
8	Augment 4	Birch	420	12.5 mm	6.9	1-2	20
9	Minimum Temp	Birch	275	12.5 mm	12.4	1-2	20
10	Particle Size (CP series)	Birch	320	25 mm	0.69	< 0.2	8
11	Particle Size (CP series)	Birch	320	25 mm	12.4	< 0.2	8

Constant volume WHTB reactions

A summary of constant volume tests is shown in Table 2. Tests were all conducted at 320 °C across a range of initial reactor nitrogen pressures from 0 to 2.0 MPa. All reaction times were 30 minutes.

Author Accepted Manuscript version of the paper by Robert Johnson et al.
in ACS Sustainable Chemistry & Engineering Vol. 11 (2023) Page, DOI: http://dx.doi.org/10.1021/acssuschemeng.2c05229

Table 2: Experiments for constant volume reaction series. All reaction times were 30 minutes.

Biomass	Temperature (°C)	Reactor	Initial Pressure (MPa)	Max Pressure (MPa)	Particle Size (mm)	H_2O wt %
Birch	**320**	**25 mm**	**0**	**7.07**	**1-2**	**8**
Birch	**320**	**25 mm**	**0.55**	**7.72**	**1-2**	**8**
Birch	**320**	**25 mm**	**1.1**	**10.45**	**1-2**	**8**
Birch	**320**	**25 mm**	**2.0**	**12.4**	**1-2**	**8**

Calcination (N_2) of biochar to produce biocarbon pellets

Biochar pellets (6 mm diameter, forming process described below) were formed from 0.5 to 1.0 mm particles under 168 MPa pressure. After weighing, pellets were devolatilized in a 25 mm quartz tube furnace at a rate of 1 °C/min to 900 °C, held for 1 hr, then passively cooled. 1.6 L/min of nitrogen (Matheson Tri-Gas, Ultra-High Purity, 99.999% purity) flowed through a trap (Restek, RES-20601) rated to remove oxygen below 20 ppb and then purged the quartz tube. Following devolatilization, the mass of the pellets was determined and the dimensions measured using a micrometer (Mintoya Corp., Model CD-6"C, ±5 μm).

Analytical Methods

Analytical methods used for biochar and biocarbon analysis are described in the following sections.

Proximate analysis

Author Accepted Manuscript version of the paper by Robert Johnson et al.
in ACS Sustainable Chemistry & Engineering Vol. 11 (2023) Page, DOI: http://dx.doi.org/10.1021/acssuschemeng.2c05229

Moisture content, volatile matter, fixed carbon and ash of the biocarbon produced from the WHTB reactor were determined using a LECO TGA801 System with operating conditions as specified by the manufacturer for proximate analysis. All samples were run in triplicate with ~1 g of sample used for each replicate. The LECO TGA 801 program is provided in the supplementary information (Figure S2).

Helium pycnometry

True density measurements were conducted using a pycnometer (Anton-Parr Ultrapyc 5000) with a helium atmosphere (Matheson Tri-gas, Research Grade, 99.9999% purity). The system was run at 20 °C and 0.1 MPa in "reference cell mode" to avoid system contamination by fine powder present in the sample. Samples were run for a minimum of 25 measurements and the average of the last five measurements are reported. Graphite powder (true density 2.26 g/cm^3) and ammonium ZSM-5 zeolite (National Institute of Standards and Technology, Reference Material 8852, 2.35 g/cm^3) [30] with known true densities were used to verify the accuracy of the system. Plots of several runs are shown in supplementary information (Figures S3,4).

Universal tester

Biochar powder compaction experiments were conducted using a universal tester, (Shimadzu, model AGS-X) equipped with a 5 kN load cell (±1% from 10-5000 N) with Trapezium software (version 1.5.6) and a 6 mm diameter die (Precision Elements Ltd, Traverse City, MI) made from D2 tool steel.

Pellets were formed in the die using a piston travel speed of 10 mm/min to reach the target maximum force and then held for 120 sec. The measurement start point in the compression program was defined at a force of 20 N. The piston travel distance, the height of the pellet at the end of the compression stroke (under load in the die), and the height and diameter of the pellet after removal from the die and immediately before tensile strength determination were recorded for each sample.

Author Accepted Manuscript version of the paper by Robert Johnson et al.
in ACS Sustainable Chemistry & Engineering Vol. 11 (2023) Page, DOI: http://dx.doi.org/10.1021/acssuschemeng.2c05229

Tensile strength was determined using diametric compression of cylindrical pellets with a piston travel speed of 1 mm/min, and calculated using equation (5), where F is the measured force and D_o is the initial diameter. Curves for tensile tests are shown in (Figures S5-7).

The tensile modulus, E, was determined using the max slope function and a 250 point fit in the Trapezium software. The force-displacement slope (N/mm) obtained in Trapezium was converted into stress vs strain (N/mm^2 = MPa) using equations 5 and 6.

$$\sigma = Stress = \frac{2F}{\pi * Do * H} \quad (5)$$

$$e = Strain = \frac{D - Do}{Do} \quad (6)$$

$$E = \frac{\sigma}{e} = \frac{F}{D - Do} * \frac{2}{\pi H} = [slope] * \frac{2}{\pi * H} \quad (7)$$

The thermal expansion of the TPPB and NTPPB pellets was determined by placing pellets into a furnace (air) at 100, 150, 200 ^{o}C for 1 hour and measuring the diameter and radius using a micrometer.

Scanning electron microscopy (SEM)

SEM micrographs were obtained using a JOEL JSM 5900LV SEM with a working distance of 18 mm with corresponding voltage of 15 kV and spot size of 24.

^{13}C NMR

NMR spectra of TPPB samples were acquired at the Chemical Instrumentation Facility at Iowa State University using a Bruker Avance 400 under a 9.6 T field corresponding to Lamor frequencies for ^{1}H of 400.13 MHz and 100.62 MHz for ^{13}C. A 4 mm three channel probe was run in double resonance mode with a MAS frequency of 14 kHz using 62.5 kHz TPPM ^{1}H decoupling. Cross polarized spectra were acquired using 50 kHz power on ^{13}C with a ^{1}H sideband match condition with a cross polarization period of 5 ms. Direct polarized (DP) spectra were acquired with a recycle delay of 50 s and 3 k scans.

Author Accepted Manuscript version of the paper by Robert Johnson et al.
in ACS Sustainable Chemistry & Engineering Vol. 11 (2023) Page, DOI: http://dx.doi.org/10.1021/acssuschemeng.2c05229

Thermogravimetric analysis (TGA)

TGA was carried out using a TA Instruments TGA 5500 under a 50 ml/min flow of ultra-high purity N_2. The heating program ramped 10 ^oC/min to 110 ^oC with a 30 minute hold to evaporate all residual moisture followed by a 10 ^oC/min ramp to 1100 ^oC.

Results and Discussion:

Results of the tests summarized in Tables 1 and 2 are described below.

Influence of pressure on TPPB formation – Experiments 1 - 5 and 10/11 in Table 1

Figure 1A shows the visual changes in the material morphology as a function of pressure. No TPPB formation was observed under pressures of 0, 0.69, and 4.48 MPa, minor TPPB formation was observed at 6.89 MPa, and complete TPPB formation occurred at 10.3 MPa. Minimal differences in solid and fixed carbon content were observed as a function of pressure (Figure 1B), despite seeing drastic changes in the material morphology. If TPPB resulted from secondary char formation around individual primary biochar particles, differences in the solid yield and potentially fixed carbon content would be expected; these differences are not observed. Particles in a size range of 1-2 mm were selected for two reasons. First, larger particles have a larger void space than a fine powder, and the formation of TPPB is much more apparent. Second, pyrolysis reactions under constant pressure conditions release gas from the system upon heating in the sand bath. Effectively this outgassing would not be favorable for TPPB to form if the primary mechanism was secondary charcoal formation.

Author Accepted Manuscript version of the paper by Robert Johnson et al.
in ACS Sustainable Chemistry & Engineering Vol. 11 (2023) Page, DOI: http://dx.doi.org/10.1021/acssuschemeng.2c05229

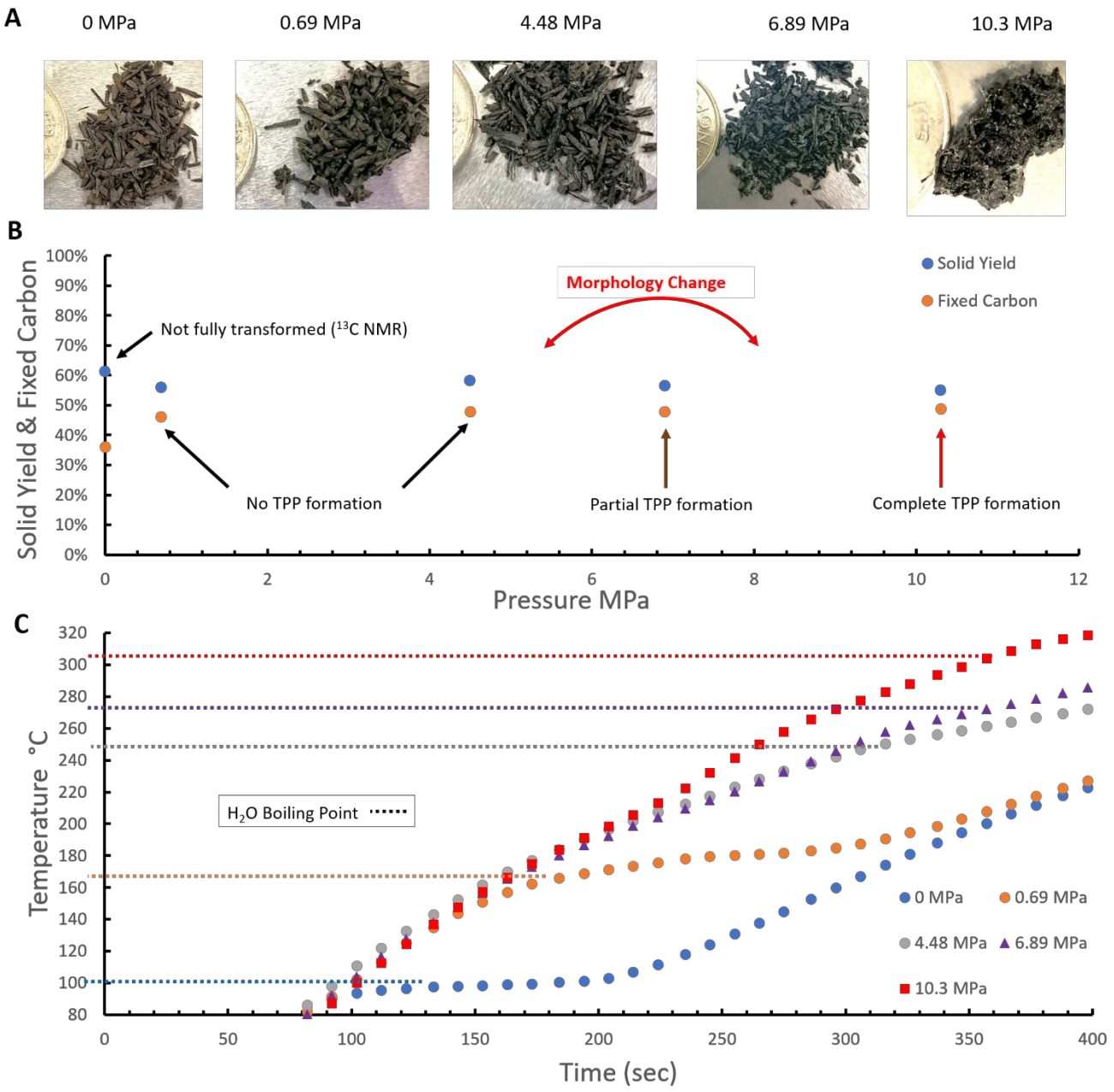

Figure 1: (A) Photographic results from 1-2 mm birch particles following constant pressure carbonization experiments at 320 °C for 30 mins, (B) Solid yield and fixed carbon content as a function of pressure and (C) Heating profiles from constant pressure pyrolysis with 1-2 mm birch particles reacted at 320 °C for 30 min. (TPP = transient plastic phase)

Author Accepted Manuscript version of the paper by Robert Johnson et al.
in ACS Sustainable Chemistry & Engineering Vol. 11 (2023) Page, DOI: http://dx.doi.org/10.1021/acssuschemeng.2c05229

The temperature profiles for each of the test conditions are shown in Figure 1 (C). Lower reactor pressures display a prominent endotherm occurring near the corresponding boiling point of water (dashed horizontal line). Under conditions that formed TPPB, the temperature profile steepens at ~210 ^{o}C where the profiles of the three highest pressure experiments diverge. Additionally, the boiling point of water at 6.9 MPa is 275 ^{o}C, and therefore if TPPB formation is water mediated melting, we would expect the temperature required for this to occur would be > 275 ^{o}C. Results from tests run with a fine powder were consistent with respect to TPPB formation.

TPPB molten phase validation

The partitioned reactor shown in (Figure S8) produced a TPPB solid (Table 1, test 6) that had undergone a drastic morphology transformation with 62% of the dry product mass recovered below the 1 mm screen and the remaining 38% above. The screen was plugged with material with the same morphology as the contents of the lower reactor. Moreover, the material that did not pass through the 1 mm screen was accumulated as a solid chunk piled atop the screen. The only plausible explanation for the test results (product location and form) is that the biomass feedstock passed through a molten phase during the course of the reaction. An additional experiment was run under NTPPB formation conditions (0.69 MPa, 320 °C, 30 min) and as expected the biochar retained the parent particle morphology and 100% of the solid product mass was recovered from above the screen.

Temperature effect on TPPB formation, Tests 4 and 8

Results from Table 1, Test 8 conditions produced a biochar product that showed only partial TPPB formation, comparable to the product from test 4. Tests 4 and 5 as a pair demonstrate that increased pressure can shift biochar characteristics from a partial TPPB product to a fully agglomerated TPPB product. Test 4 and 8 as a pair demonstrate that an increase in temperature of 100 °C does not produce a comparable effect on biochar product characteristics. Taken together, this suggests that a minimum pressure is required for TPPB to form, which likely is related to the boiling point of water.

Minimum temperature requirement for TPPB formation

Author Accepted Manuscript version of the paper by Robert Johnson et al.
in ACS Sustainable Chemistry & Engineering Vol. 11 (2023) Page, DOI: http://dx.doi.org/10.1021/acssuschemeng.2c05229

After establishing the lower pressure range required for TPPB formation, identifying a lower temperature limit was also of interest. Temperature >275 °C can be inferred from the constant pressure experiment results (See Figure 2). Test 9 temperature, 270 °C, corresponds to the boiling point of water at 6.89 MPa (see Figure 2). Under these conditions TPPB formation was not observed, suggesting a minimum temperature greater than 275 °C is required for TPPB formation with a 30 min reaction time. These results corroborate the conclusions drawn from the water-boiling point curves and TPP formation from the constant pressure series. Taken together, it appears that the reactions responsible for TPPB formation have an activation energy threshold above 275 °C for the range of test parameters summarized in Table 1.

Constant volume experiments with different initial pressure

TPPB formation was initially observed from constant volume reactor conditions which resulted in elevated pressures [18]. Although, the role of pressure is somewhat more complicated to investigate since the pressure is changing with temperature as the reaction proceeds. In addition, there is no loss of material as with the constant pressure experiments. Therefore, it is unclear if the TPPB formation conditions required under constant pressure would be transferable for TPPB formation under constant volume conditions. To compare the required conditions for TPPB formation between constant pressure and constant volume a series of constant volume tests were conducted (Table 2). Results from constant volume experiments (Figure 2A) show that initial pressures of 1.1 and 2.0 MPa lead to TPPB formation, whereas initial gage pressures of 0 and 0.56 MPa did not lead to TPPB formation. To evaluate these results on a similar basis, constant pressure experiments' reactor temperature-pressure profiles were plotted with the boiling point of water as a function of temperature. (Figure 2B) The two conditions forming TPPB (indicated as squares) resulted in reactor pressures above the water boiling point up to 290 °C where the 1.1 MPa curve crosses the saturated liquid line. The NTPPB sample with initial pressure of 0.56 MPa crossed the water boiling point curve at 265 °C. Under constant pressure conditions, birch formed TPPB via a water-mediated hydrolysis-melting above 275 °C. The temperature pressure profiles from the constant volume experiments support the conclusions from the constant pressure experiments.

Author Accepted Manuscript version of the paper by Robert Johnson et al.
in ACS Sustainable Chemistry & Engineering Vol. 11 (2023) Page, DOI: http://dx.doi.org/10.1021/acssuschemeng.2c05229

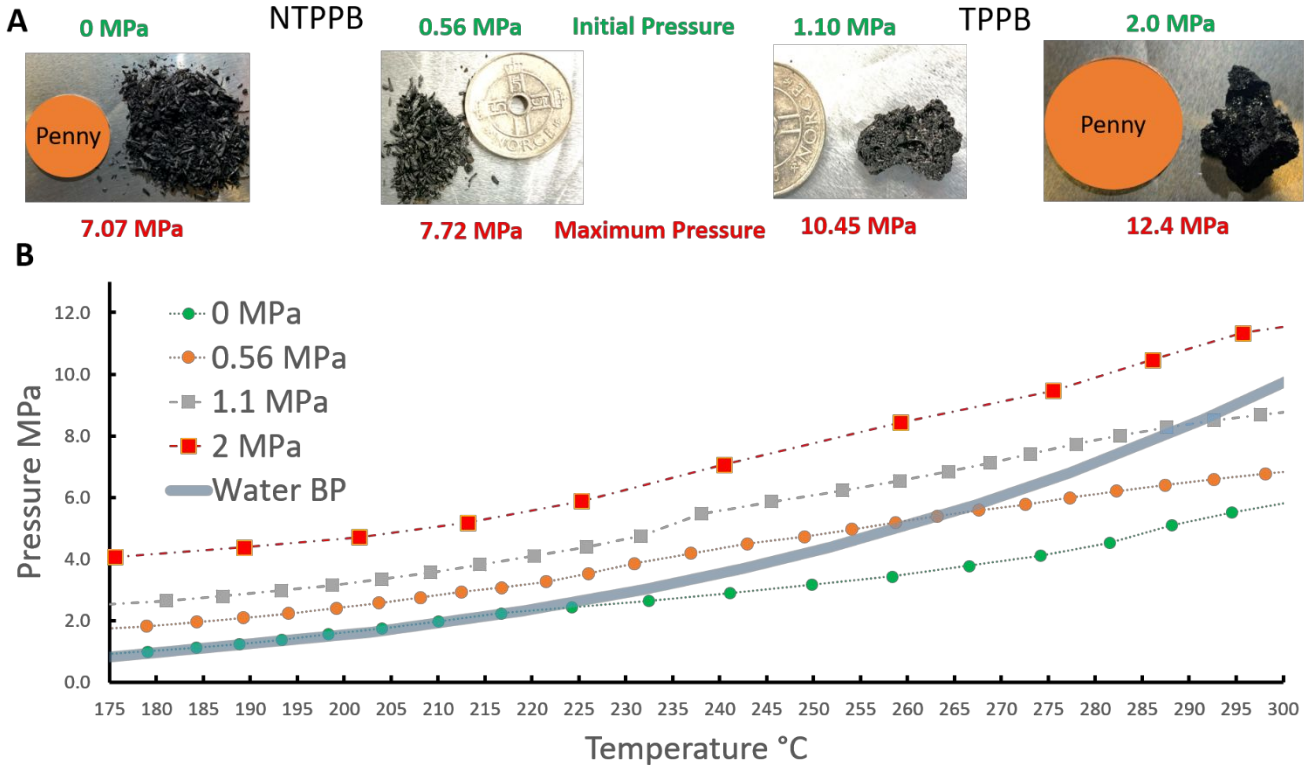

Figure 2: Results of constant volume experiments with 1-2 mm birch particles at 320 °C for 30 min reaction times: (A) initial and maximum pressures and photos of products, and (B) reactor temperature vs pressure profiles for initial reactor test pressures overlaid with the saturated liquid, pressure-temperature curve for water (Water BP). (Note: TPPB = transient plastic phase biochar and NTPPB = non transient plastic phase biochar).

Figure 3 compares the char yields and fixed carbon contents from birch for all the constant pressure and constant volume experiments that were conducted at 320 °C. Across the range of maximum reactor pressures, char yields vary from 53% at the maximum constant volume pressure of 12.4 MPa to 61% for the constant atmospheric pressure conditions. The latter reaction conditions produced a fixed carbon biochar content of 36%. Above 0.69 MPa reactor pressures, fixed carbon contents ranged from 48 to 51%.

Author Accepted Manuscript version of the paper by Robert Johnson et al.
in ACS Sustainable Chemistry & Engineering Vol. 11 (2023) Page, DOI: http://dx.doi.org/10.1021/acssuschemeng.2c05229

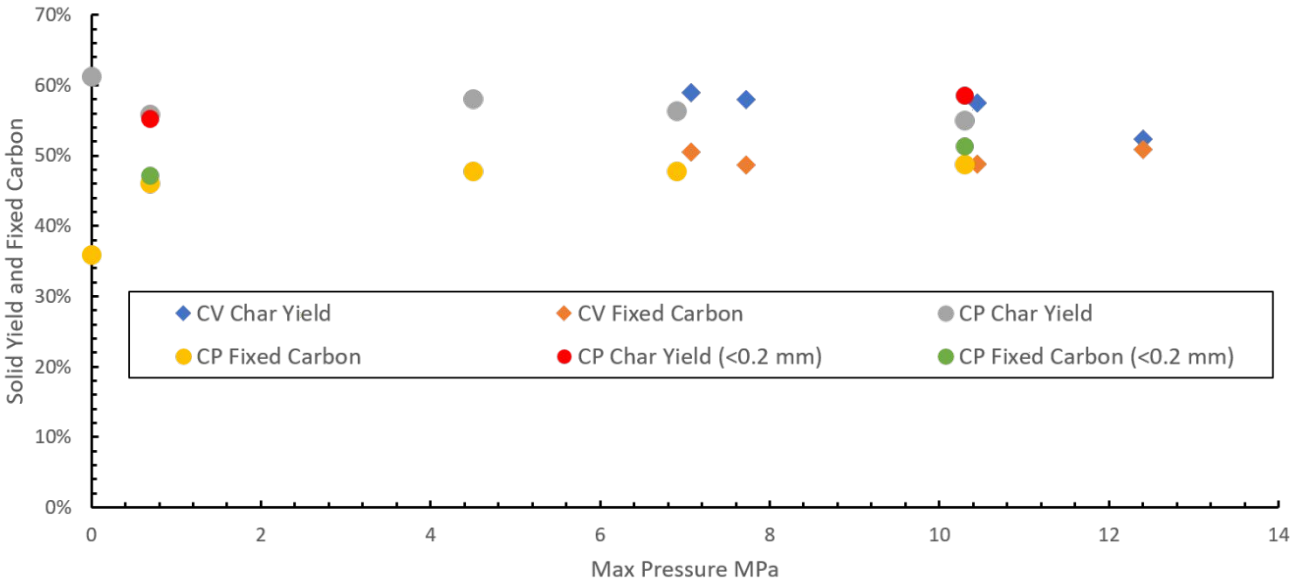

Figure 3: Comparison of char yield and fixed carbon for all constant volume (CV) and constant pressure (CP) experiment with 1-2 mm and <0.2 mm birch particles pyrolyzed at 320 °C for 30 minutes.

True density determination via helium pycnometry

Measured true densities of NTTPB and TPPB materials are shown in (Figure S9). The fresh NTPPB material had a greater true density of 1.31±0.05 compared to 1.21±0.05 g/cc for TPPB when the measurement is made on material directly recovered from the reactor. After cryomilling the material into a fine powder the measured true densities are nearly identical 1.35±0.002 g/cc. These results show that the TPPB and NTPPB have effectively the same true densities, suggesting the chemical compositions are similar. The change in the measured true density of the milled TPPB material indicates the presence of gas-inaccessible pore space equal to ~10% of the TPPB volume, a finding consistent with the occurrence of a molten phase during pyrolysis. Therefore, an observed change in true density measured as a function of particle size provides a non-quantitative measure of the pore accessibility of the material. Known true densities of other SP^2 hybridized carbon materials have an upper limit of 2.34 g/cc for crystalline graphite, and lower limits of 1.5 g/cc for glassy carbon, with intermediate densities for calcined petroleum cokes ranging from 1.8-2.2 g/cc. The low true densities of the TPPB and NTPPB materials

Author Accepted Manuscript version of the paper by Robert Johnson et al.
in ACS Sustainable Chemistry & Engineering Vol. 11 (2023) Page, DOI: http://dx.doi.org/10.1021/acssuschemeng.2c05229

reflects the high oxygen content and underdeveloped degree of polycondensation that occurs with higher temperature thermochemical reactions.

The true densities of cryomilled biochar from the constant pressure series (Table 1, Tests 1-5) were also measured. In keeping with the proximate analyses of these samples reported in (Figure S10), no differences between the measured true densities are evident across pyrolysis pressures. The average for the five values across the pressure range is 1.33 g/cc with a standard deviation of 0.01 g/cc. Lastly, the measured true densities of the constant volume experiments (Table 2) averaged 1.35 g/cc with a standard deviation of 0.002, indicating little difference between the constant volume and constant pressure series. The results from helium pycnometry support the conclusions that TPPB and NTPPB have minimal differences at the chemical level, although the apparent difference in accessible pore space confirms a morphological change has occurred.

Solid state ^{13}C NMR

Solid state ^{13}C NMR quantitatively identifies functional groups present in samples. Analysis of chars and humic materials is difficult because numerous overlapping aromatic peaks are present. Extensive work using advanced NMR techniques has dramatically improved the understanding of average chemical structures present in low temperature char materials. [14-16, 31-34] To compare functional groups of TPPB and NTPPB, semi-quantitative ^{13}C cross-polarized spectra (Figure 8) were obtained using a long cross polarized spin transfer time (5 ms). Although these simple spectra do not provide sufficient information to determine average molecular structures, differences between TPPB and NTPPB can be assessed. Spectra in Figure 4A show no detectable differences in the prominent peak locations, and the relative intensity of major peaks. This demonstrates that the two materials have minimal differences in average chemical structures. Both spectra lack residual intensity characteristic of alkyl OCH groups present as carbohydrates in the parent biomass, indicating that both materials have been significantly transformed. Both spectra are dominated by sp^2 hybridized carbon in the form of furanic and phenolic species that contain a large fraction of O-CH_3 groups. Both spectra exhibit a large aromatic peak area that reflects a

Author Accepted Manuscript version of the paper by Robert Johnson et al.
in ACS Sustainable Chemistry & Engineering Vol. 11 (2023) Page, DOI: http://dx.doi.org/10.1021/acssuschemeng.2c05229

mixture of lignin and furanic products, and the characteristic $C_{aromatic}$-O one (150-165 ppm) and two bonds (100-110 ppm) from oxygen. The alkyl region of the spectra has a sharp OCH_3 peak at 55 ppm corresponding to methoxy groups present on lignin. A sharp CH_2 peak at 30 ppm and ketone at 205 ppm reflect levulinic acid. CH_3-COO groups cause the sharp CH_3 peak at 21 ppm characteristic of acetic acid and/or acetate. These results show that the materials are not drastically different despite the huge difference in morphology. Figure 4B compares the cross polarized spectra for the native birch wood, and DP spectra for the constant atmospheric pressure (Table 1 test 1) and the constant pressure TPP sample (Table 1 test 5). Incomplete thermochemical transformation in the atmospheric sample is evident from significant intensity of alkyl CO peaks characteristic of cellulose in biomass in the 60 to 110 ppm range. The TPPB CP and DP spectra deviate only minimally, and verify the CP conditions are adequate to obtain an accurate spectra.

Author Accepted Manuscript version of the paper by Robert Johnson et al.
in ACS Sustainable Chemistry & Engineering Vol. 11 (2023) Page, DOI: http://dx.doi.org/10.1021/acssuschemeng.2c05229

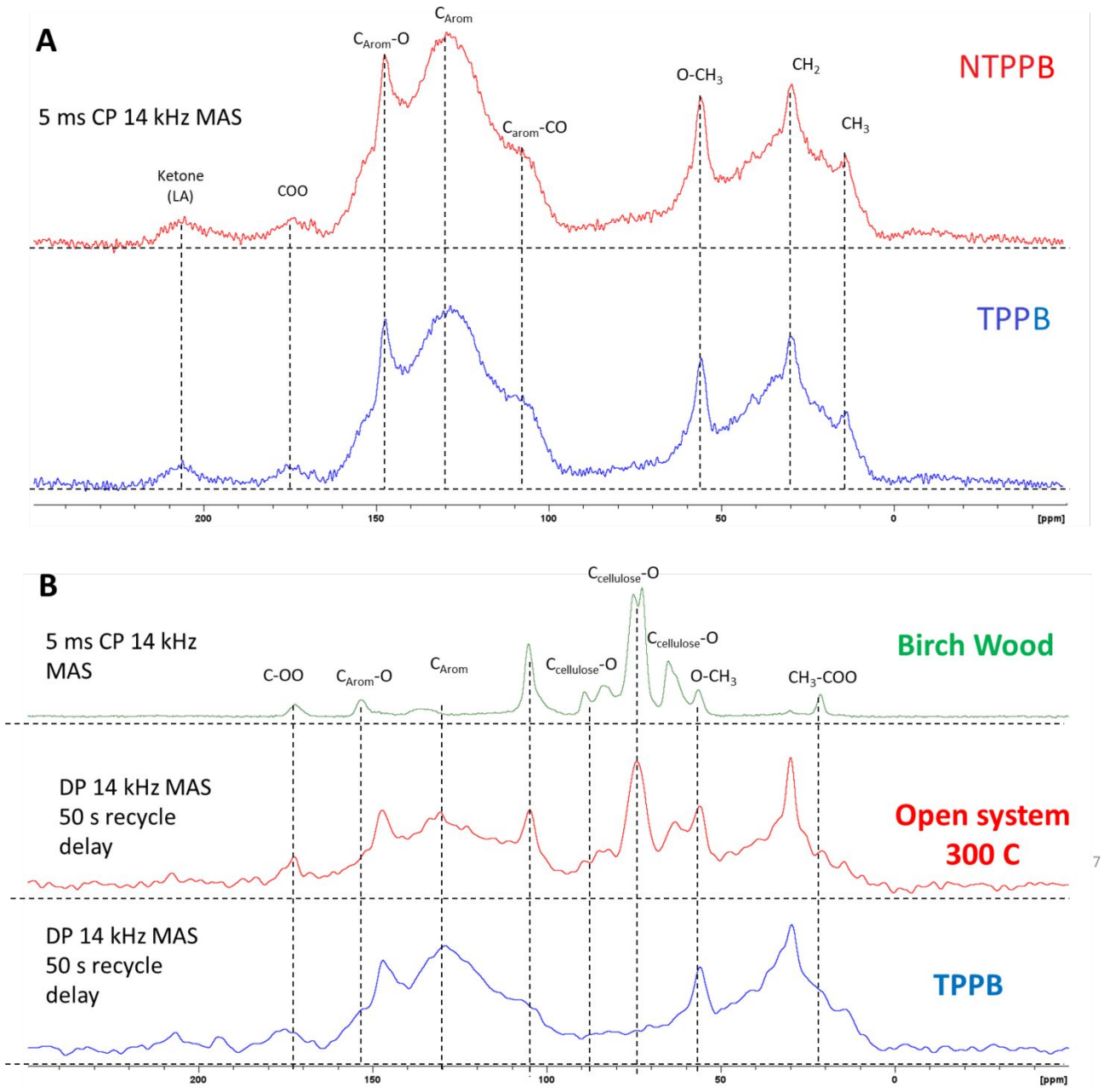

Figure 4: Shown in (A) are 5 ms ^{1}H-^{13}C cross-polarized spectra acquired with 14 kHz MAS frequency from TPPB and NTPPB materials obtained from constant volume experiments. Shown in (B) are a comparison of birch wood cross polarized spectra to direct polarized spectra from TPPB (ID-5) and the NTPPB (ID-1) acquired using 50 s recycle delay and 3 k scans. (Note: TPPB = transient plastic phase biochar and NTPPB = non transient plastic phase biochar).

Author Accepted Manuscript version of the paper by Robert Johnson et al.
in ACS Sustainable Chemistry & Engineering Vol. 11 (2023) Page, DOI: http://dx.doi.org/10.1021/acssuschemeng.2c05229

TGA of constant pressure biochars

TGA results (Figure S11) show a clear trend of increased mass loss with increasing pressure between 200 and 400 ^{o}C and an increase of temperature where maximum loss occurs. This is consistent with the higher-pressure TPPB samples being depolymerized after passing through a molten phase.

Characterization of TPPB and NTPPB powders

Considering that techniques sensitive to chemical level differences showed minimal differences between TPPB and NTPPB, the need for a technique to characterize macromolecular properties is apparent. The compressibility profiles of TPPB and NTPPB using small (0.075-0.15 mm) and large (0.5-1 mm) particle size fractions show the two materials behave drastically different (Figure 5A). The TPPB solid fraction at 166 MPa approaches nearly 80% compared to the NTPPB which is below 60%. The difference in the response is greater at 53 MPa with solid fractions of TPPB being 68% and NTPPB being 42%. Differences are also reflected by the minimum pressure required to form a stable pellet, with TPPB forming a stable pellet with as little as 8.8 MPa pressure, compared to 53 MPa required for the NTPPB material. The compressibility profiles of the two TPPB particle size classes are identical, whereas the NTPP values differ by ~3% (absolute) with the smaller size class having a higher solid fraction. These differences indicate that the TPPB material undergoes plastic deformation and/or fracture to a far greater extent than NTPPB. This mechanical response would be consistent with TPPB having undergone a molten phase, that would result in a breakdown of the macromolecular structure of the parent material.

Author Accepted Manuscript version of the paper by Robert Johnson et al.
in ACS Sustainable Chemistry & Engineering Vol. 11 (2023) Page, DOI: http://dx.doi.org/10.1021/acssuschemeng.2c05229

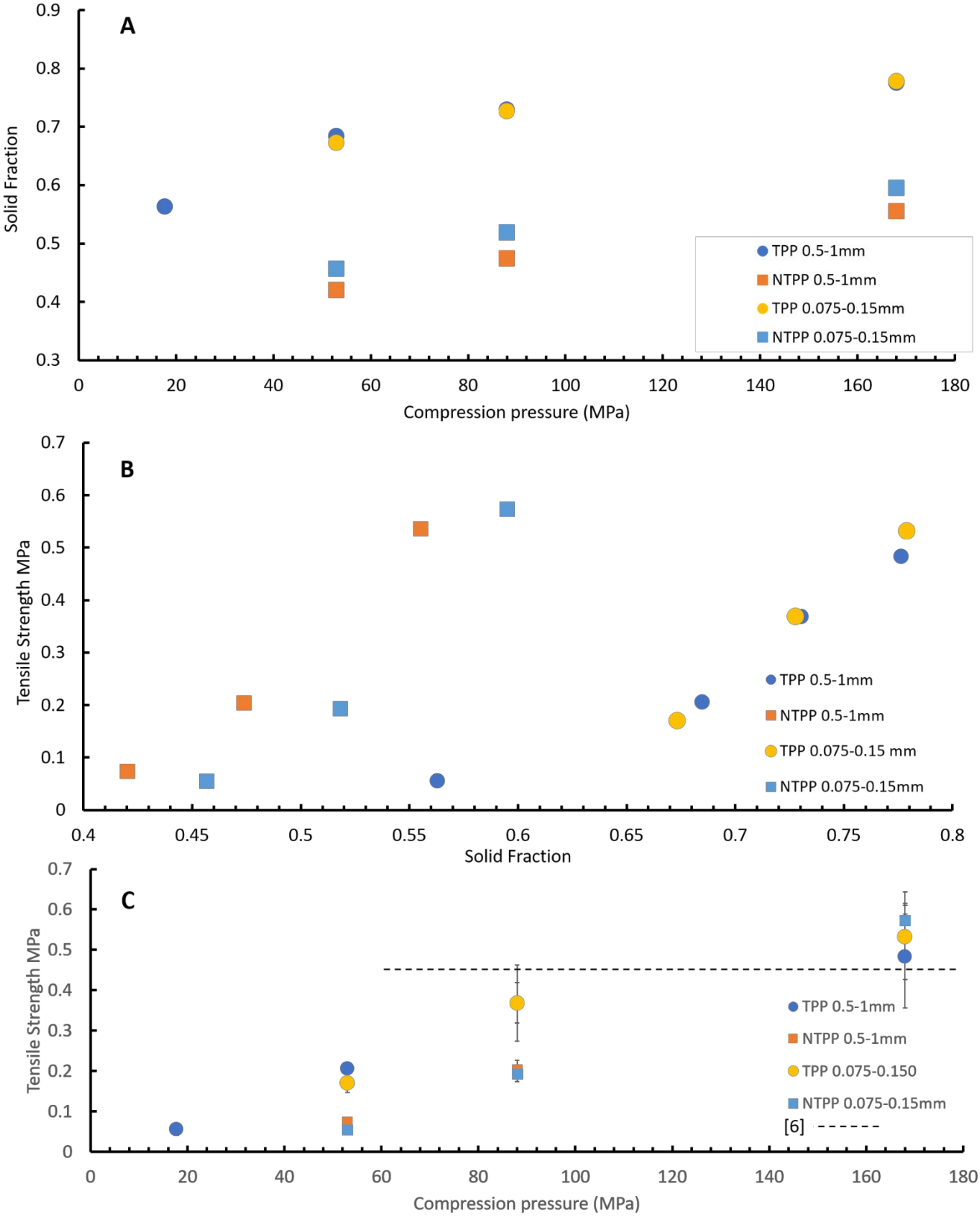

433

Author Accepted Manuscript version of the paper by Robert Johnson et al.
in ACS Sustainable Chemistry & Engineering Vol. 11 (2023) Page, DOI: http://dx.doi.org/10.1021/acssuschemeng.2c05229

Figure 5: (A) Compressibility profiles of two size classes of TPPB and NTPPB powders formed into 6 mm pellets across a range of piston loading pressures. (B) : Compaction profile of two size classes of TPPB and NTPPB powders formed into 6 mm pellets. (C) Tabletability profile of two size classes of TPPB and NTPPB powders formed into 6 mm pellets across a range of piston loading pressures. (Note: TPP = transient plastic phase and NTPP = non transient plastic phase). *Dotted line represents highest value for bio-oil (30 wt%) − biochar (70 wt%) pellet pressed at 60 ^{o}C). [10]

The compactability profiles for TPPB and NTPPB pellets from the same two particle size fractions are shown in Figure 5B. These plots show that their maximum tensile strengths (0.5 to 0.6 MPa) are comparable at their highest solid fractions. At 0.55 to 0.6 solid fractions, NTPPB has an order of magnitude higher tensile strength. This behavior would be consistent with TPPB having a greater inter-particle bonding area, but lower bonding strength and NTPPB having greater bonding strength and lower bonding area. This would be consistent with NTPPB material retaining its structural integrity, and the associated strength.

The tabletability profiles for TPPB and NTPPB pellets from the same two particle size fractions are shown in Figure 5C. TPPB pellets exhibit greater tensile strength than NTPPB pellets at low pressures and asymptotically approach a common 0.5 to 0.6 MPa range at compression pressures of 168 MPa reflecting the increased bonding area between particles. The NTPPB pellet profiles exhibit a linear increase in tensile strength with increasing pressure from 53 and 168 MPa. This reflects how NTPPB is resistant to plastic deformation and fracture compared to TPPB, allowing for additional bonding area to develop with higher pressures.

Data from the compressibility, compactability, and tabletability profiles suggests that NTPPB is much more resistant to fracture and plastic deformation compared to TPPB. This would be apparent from greater volume expansion of pellets after compressive loads are removed. The change in volume after 128 hours at room temperature are shown in Figure 6 as a function of compression pressure for TPPB and NTPPB pellets. These data show that at all pressures the NTPPB expands to a far greater extent than the NTPPB materials. At 168 MPa the

Author Accepted Manuscript version of the paper by Robert Johnson et al.
in ACS Sustainable Chemistry & Engineering Vol. 11 (2023) Page, DOI: http://dx.doi.org/10.1021/acssuschemeng.2c05229

TPPB and NTPPB materials expanded 4% and 15%, respectively, representing nearly 4 fold greater volume expansion. This large difference in elasticity between the TPPB and NTPPB materials is consistent with the compressibility, compactability, and tabletability profiles.

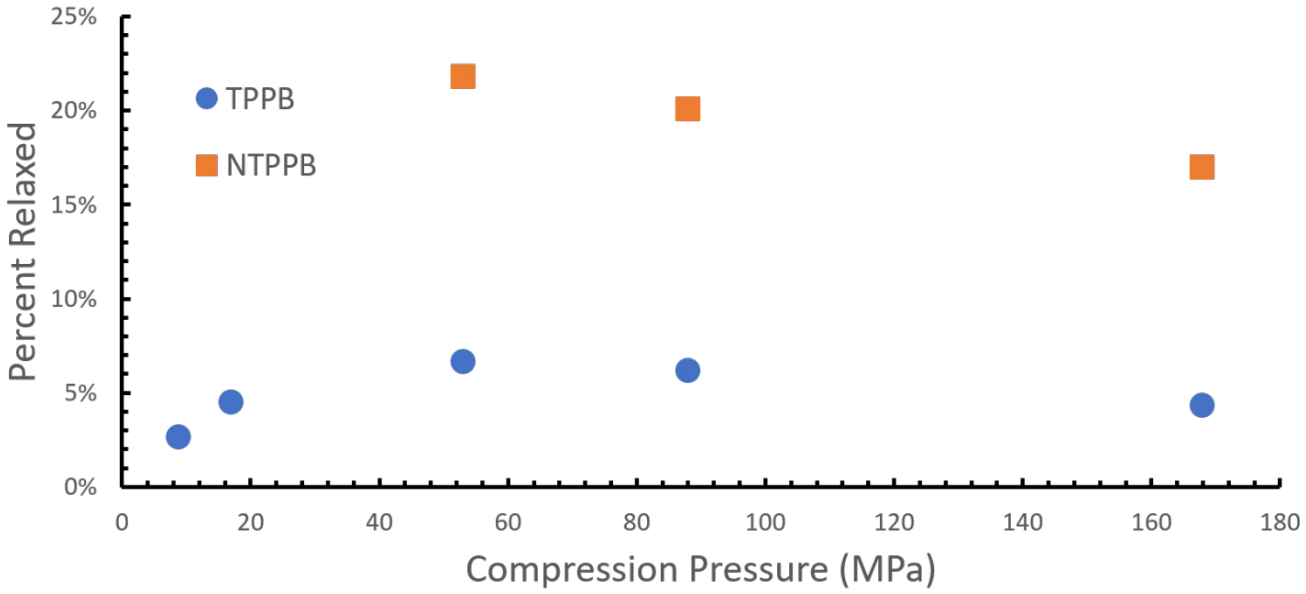

Figure 6: Comparison in volume change of 6 mm pellets of TPPB and NTPPB materials after 128 hours of relaxation. (Note: TPPB = transient plastic phase biochar and NTPPB = non transient plastic phase biochar).

Figure 7 presents a plot of the pellet tensile moduli as a function of pellet-forming pressure. At 168 MPa compression pressure TPPB has a tensile modulus of around 50 MPa compared to NTPPB at ~20 MPa. Additionally, the response of tensile modulus vs compression pressure shows TPPB has a slope nearly twice that of NTPPB. These data show that the pellets formed from TPPB are much less ductile compared to NTPPB.

Author Accepted Manuscript version of the paper by Robert Johnson et al.
in ACS Sustainable Chemistry & Engineering Vol. 11 (2023) Page, DOI: http://dx.doi.org/10.1021/acssuschemeng.2c05229

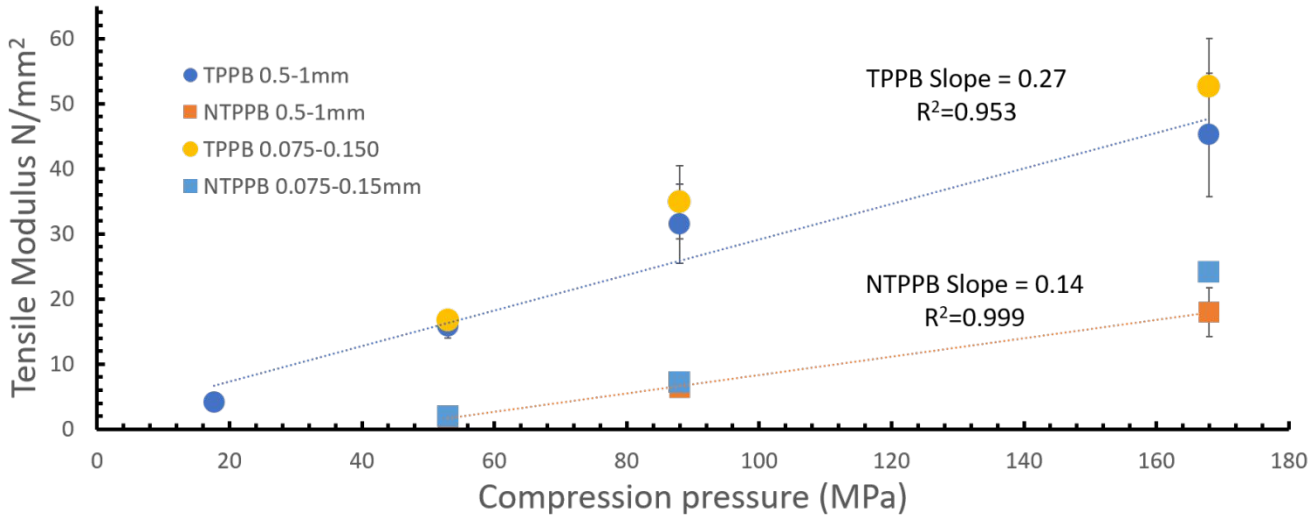

Figure 7: Tensile moduli of two size classes of TPPB and NTPPB powders formed into 6 mm pellets across a range of piston loading pressures. (Note: TPPB = transient plastic phase biochar and NTPPB = non transient plastic phase biochar).

The results for TPPB and NTPPB produced from <0.2 mm and 1 to 2 mm birch particles at the same reactor conditions are shown in Figure S12-A. Their calcined products (NTPPC and TPPC) are presented in Figure S12-B. Calcined (N_2) and un-calcined TPPB and NTPPB pellets produced from <0.2 mm birch particles exhibited reduced mechanical strength compared to their 1 to 2 mm counterparts. Calcining increased the tensile strength of the <0.2 mm and 1-2 mm size class TPPB pellets by factors of ~ 6 and 9, respectively.

Given the significant differences in mechanical properties related to compressibility and elasticity, the relative thermal expansion of TPPB and NTPPB pellets were determined; the results shown in Figure 8. The greater elasticity of NTPPB material pellets observed at room temperature was amplified when heated. After 1 hr at 200 °C the NTPPB pellet expanded by 11.5% compared to 2.5% for the TPPB pellet. These data suggest that the TPPB pellets would be more apt to maintain mechanical integrity following heating compared to the NTPPB pellets.

Author Accepted Manuscript version of the paper by Robert Johnson et al.
in ACS Sustainable Chemistry & Engineering Vol. 11 (2023) Page, DOI: http://dx.doi.org/10.1021/acssuschemeng.2c05229

Reduced thermal expansion will allow for greater intraparticle contacts to be retained and allow for formation of covalent bonds between particles to form a strong contiguous solid.

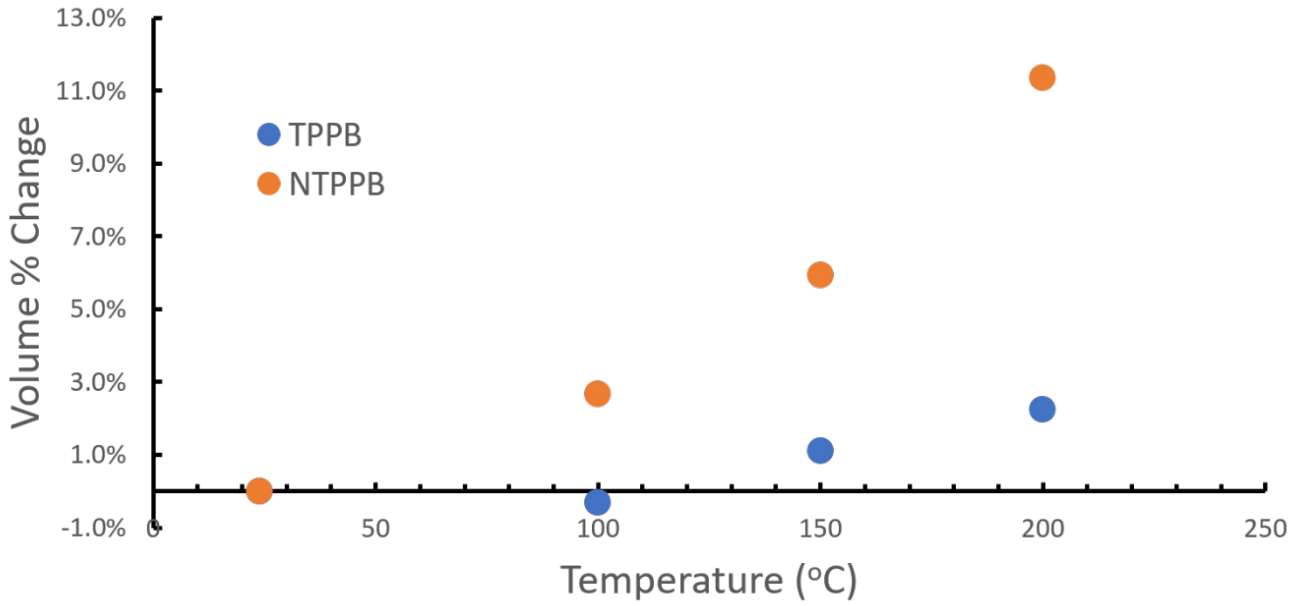

Figure 8: Change in volume of NTPPB and TPPB pellets after 1 hour exposure as a function of exposure temperature. (Note: TPPB = transient plastic phase biochar and NTPPB = non transient plastic phase biochar).

SEM of TPPB and NTPPB pellets

SEM images of TPPB pellets formed from 0.5-1 mm particles under different compression pressures at magnification of 55X, 200X and 800X are shown in (Figure S13). Images from 55X magnification support the conclusion from the compressibility profile that TPPB powders fracture and undergo plastic deformation at pressures as low at 17 MPa, as virtually no remnants of the original powder particles can be identified. Optical images of the pellets were also obtained (Figure S14) with a 0.5 mm red box shown in the figure to further highlight

Author Accepted Manuscript version of the paper by Robert Johnson et al.
in ACS Sustainable Chemistry & Engineering Vol. 11 (2023) Page, DOI: http://dx.doi.org/10.1021/acssuschemeng.2c05229

this point. As expected, the surface roughness decreases substantially with increasing compression pressures. Images from 800X magnification and low compression pressure show interesting features that resemble bubbles, which would be consistent with formation of a molten phase while gas formation was occurring. The NTPPB SEM images shown in (Figure S15) display morphology that is typical of char derived from woody biomass that retains its fibrous structural elements. Moreover, the outlines of individual particles used to form the pellets are evident, indicating that even at high pressure the degree of particle fracture and plastic deformation is much less than for TPPB material.

The SEM images are consistent with the conclusions from the powder compression experiments, showing that the pelleted TPPB material has undergone a major change in morphology consistent with having undergone a molten phase. The tabletability and compactability profiles for NTPPB and TPPB pellets provide insight into the resulting differences. NTPPB pellet strength is developed via interlocking un-fractured materials that retain the fibrous morphology which leads to a high bonding strength and low bonding area. TPPB pellets develop strength through fragmentation and plastic deformation leading to greater bonding area, but with reduced bonding strength. The powder compression experiments and SEM images indicate that TPPB should be a superior starting material to produce formed biocarbon with improved mechanical strength.

Biochar calcination (N_2) to form biocarbon

Results from the pelletization experiments show that as a result of having undergone a molten phase, TPPB pellets have a much higher solid fraction and much lower elasticity and thermal expansion. This suggests that upon further heating to convert TPPB into biocarbon TPPC, there would be greater intra particle contact, leading to greater covalent bond formation between particles resulting in a material with greater mechanical strength compared to the NTPPB material. This hypothesis was tested by devolatilizing both TPPB and TPPC (0.5-1 mm particles) pellets by heating to 900 ^{o}C.

Pellets produced from TPPB and NTPPB (0.5-1 mm particles) were calcined (N_2) at 900 ^{o}C. The calcination (N_2) temperature is near the “fixed carbon” temperature (950 °C) used in proximate analysis to measure the fixed

Author Accepted Manuscript version of the paper by Robert Johnson et al.
in ACS Sustainable Chemistry & Engineering Vol. 11 (2023) Page, DOI: http://dx.doi.org/10.1021/acssuschemeng.2c05229

carbon content. After calcination the product will contain predominantly fixed carbon and low levels of ash. Differences in the mechanical properties of TPPB and NTPPB pellets carried over to the TPPC and NTPPC pellets and were amplified (Table 3). The density of the TPPC pellets is nearly double that of NTPPC pellets, with tensile and compressive strengths that are nearly ten-fold greater. The compressive strength reported for the TPPC (17 MPa) is comparable to values reported for materials produced with bio-oil/pitch binders (22-36 MPa), [6, 12] biomass/steam exploded wood pellets (5.5-16.7 MPa), [10] coal tar pitch binders (14-35 MPa), [6, 12, 35] and a commercial "Formcoke" process (28-55 MPa). [36] Although the goal of the present study was to compare characteristics of TPPC and NTPPC materials, these unoptimized results compared with those from competing applications and market products indicate that TPP material has potential to unlock new biochar applications. Improvement of TPPC mechanical strength that may be realized by controlling pellet formation (particle size, temperature, pressure, etc.) and calcination conditions (e.g. heat rates, hold times) remain unexplored. These results verify that the molten phase breakdown of macromolecular structure results in a carbon enriched material with drastically improved mechanical properties compared to conventional biochar and demonstrate an innovative approach for engineering biocarbon properties.

Table 3: Comparison of devolatilized TPPC and NTPPC pellets.

	TPPC Density (g/cc)	**TPPC Tensile Strength (MPa)**	**TPPC Compression Strength (MPa)**	**NTPPC Density (g/cc)**	**NTPPC Tensile Strength (MPa)**	**NTPPC Compression Strength (MPa)**
Mean	1.026	4.44	17.03	0.563	0.48	1.79
Standard Dev.	0.046	1.63	1.74	0.017	0.04	0.2
n	10	5	5	6	3	3

Author Accepted Manuscript version of the paper by Robert Johnson et al.
in ACS Sustainable Chemistry & Engineering Vol. 11 (2023) Page, DOI: http://dx.doi.org/10.1021/acssuschemeng.2c05229

Converting biomass into a TPPB precursor to produce biocarbon offers several potential advantages for overall process efficiency:

- The process to form TPPB does not require drying or size reduction prior to pyrolysis, and would result in a reduction in unit operations and significant energy savings.
- Keeping water in the condensed phase avoids the energy penalty associated with the latent heat of vaporization.
- The material does not require a binder to form a strong pellet this also reduces input cost and unit operations.

Conclusions:

Pyrolysis at a minimum temperature of ~270 °C and sufficient pressure to maintain fuel-bound water as a compressed liquid caused birch stemwood feedstock to undergo a molten phase, forming TPPB. TPPB was more compressible, had greater plasticity, reduced elasticity and reduced thermal expansion compared to NTPPB formed from the same parent material. TPPB calcined in N_2 resulted in a biocarbon with 10 times higher tensile/compressive strength and two-times higher apparent density compared to calcined NTPPB. These findings provide an alternative route for improving the mechanical properties of biomass-derived, carbon materials. Overcoming this limitation may enable biocarbons displacement of fossil carbon products as metallurgical reductants, binders, electrodes, or high value specialty materials.

Supporting Information:

The supporting information is available free of charge at (please add the link)

Detailed descriptions of the reactor configuration; proximate analysis heating program, true density measurements of graphite and ZSM5 zeolites, raw data from universal tester, diagram of partitioned constant

Author Accepted Manuscript version of the paper by Robert Johnson et al.
in ACS Sustainable Chemistry & Engineering Vol. 11 (2023) Page, DOI: http://dx.doi.org/10.1021/acssuschemeng.2c05229

pressure reactor, true density values for TPPB and NTPPB materials, thermogravimetric data for materials from constant pressure series, tensile strength of materials produced from different sized feedstock particles, and optical and SEM images of pellets produced from TPPB and NTPPB materials.

Acknowledgments:

The authors acknowledge the financial support from the Research Council of Norway and the BioCarbUp project industry partners: Elkem AS - Department Elkem Technology, Eramet Norway AS, Norsk Biobrensel AS, Eyde Cluster, Hydro Aluminium AS, and Alcoa Norway ANS. Additional support for the project was provided by the Office of Naval Research under grant number N-00014-18-1-2127. Solid state NMR spectra was obtained from the Chemical Instrumentation facility at Iowa State University, with special consideration to Dr. Sarah Cady for acquiring this spectra.

References:

(1) Elkasabi, Y.; Mullen, C. A. Progress on biobased industrial carbons as thermochemical biorefinery coproducts. *Energy & Fuels* **2021,** 35, 5627-5642. doi: https://doi.org/10.1021/acs.energyfuels.1c00182

(2) Uskoković, V. A historical review of glassy carbon: Synthesis, structure, properties and applications. *Carbon Trends* **2021,** 5, 100116-100148. doi: https://doi.org/10.1016/j.cartre.2021.100116

(3) Sharma, S. Glassy carbon: A promising material for micro- and nanomanufacturing. *Materials (Basel)* **2018,** 11, 1857-1878. doi: https://doi.org/10.3390/ma11101857

Author Accepted Manuscript version of the paper by Robert Johnson et al.
in ACS Sustainable Chemistry & Engineering Vol. 11 (2023) Page, DOI: http://dx.doi.org/10.1021/acssuschemeng.2c05229

(4) Hu, B.; Wang, K.; Wu, L.; Yu, S.-H.; Antonietti, M.; Titirici, M.-M. Engineering carbon materials from the hydrothermal carbonization process of biomass. *Adv. Mater.* **2010,** 22, 813-828. doi: https://doi.org/10.1002/adma.200902812

(5) Bonijoly, M.; Oberlin, M.; Oberlin, A. A possible mechanism for natural graphite formation. *Int. J. Coal Geol.* **1982,** 1, 283-312. doi: https://doi.org/10.1016/0166-5162(82)90018-0

(6) Hussein, A.; Picard, D.; Alamdari, H. Biopitch as a binder for carbon anodes: Impact on carbon anode properties. *ACS Sustain. Chem. Eng.* **2021,** 9, 4681-4687. doi: https://doi.org/10.1021/acssuschemeng.1c00618

(7) Lu, Y.; Hussein, A.; Li, D.; Huang, X.; Mollaabbasi, R.; Picard, D.; Ollevier, T.; Alamdari, H. Properties of bio-pitch and its wettability on coke. *ACS Sustain. Chem. Eng.* **2020,** 8, 15366-15374. doi: https://doi.org/10.1021/acssuschemeng.0c06048

(8) Coutinho, A. R.; Rocha, J. D.; Luengo, C. A. Preparing and characterizing biocarbon electrodes. *Fuel Process. Technol.* **2000,** 67, 93-102. doi: https://doi.org/10.1016/S0378-3820(00)00091-6

(9) Elkasabi, Y.; Darmstadt, H.; Boateng, A. A. Renewable biomass-derived coke with texture suitable for aluminum smelting anodes. *ACS Sustain. Chem. Eng.* **2018,** 6, 13324-13331. doi: https://doi.org/10.1021/acssuschemeng.8b02963

(10) Riva, L.; Nielsen, H. K.; Skreiberg, Ø.; Wang, L.; Bartocci, P.; Barbanera, M.; Bidini, G.; Fantozzi, F. Analysis of optimal temperature, pressure and binder quantity for the production of biocarbon pellet to be used as a substitute for coke. *Appl. Energy* **2019,** 256, 113933-113949. doi: https://doi.org/10.1016/j.apenergy.2019.113933

(11) Sommerseth C., D. O., Oye B., Store A., Rorvik S. . Charcoal and use of green binder for use in carbon anodes in the aluminium industry. *Light Met.* **2020,** The Minerals, Metals & Materials Series, doi: https://doi.org/10.1007/978-3-030-36408-3_183

Author Accepted Manuscript version of the paper by Robert Johnson et al.
in ACS Sustainable Chemistry & Engineering Vol. 11 (2023) Page, DOI: http://dx.doi.org/10.1021/acssuschemeng.2c05229

(12) Lu, Y.; Hussein, A.; Lauzon-Gauthier, J.; Ollevier, T.; Alamdari, H. Biochar as an additive to modify biopitch binder for carbon anodes. *ACS Sustain. Chem.Eng.* **2021,** 9, 12406-12414. doi: https://doi.org/10.1021/acssuschemeng.1c04941

(13) Lovel, R. R., de Varies, M. . A process for producing a carbonaceous product from biomass. *World Intellectual Property Organization Patent Application* **2011,** WO201114916

(14) Anderson, J. M.; Johnson, R. L.; Schmidt-Rohr, K.; Shanks, B. H. Solid state nmr study of chemical structure and hydrothermal deactivation of moderate-temperature carbon materials with acidic SO_3H sites. *Carbon* **2014,** 74, 333-345. doi: https://doi.org/10.1016/j.carbon.2014.03.041

(15) Brewer, C. E.; Schmidt-Rohr, K.; Satrio, J. A.; Brown, R. C. Characterization of biochar from fast pyrolysis and gasification systems. *Environ. Prog. Sustain. Energy* **2009,** 28, 386-396. doi: https://doi.org/10.1002/ep.10378

(16) Johnson, R. L.; Anderson, J. M.; Shanks, B. H.; Fang, X.; Hong, M.; Schmidt-Rohr, K. Spectrally edited 2D ^{13}C-^{13}C nmr spectra without diagonal ridge for characterizing ^{13}C-enriched low-temperature carbon materials. *J. of Mag. Reson.* **2013,** 234, 112-124. doi: https://doi.org/10.1016/j.jmr.2013.06.006

(17) Barin, G. B.; de Fátima Gimenez, I.; da Costa, L. P.; Filho, A. G. S.; Barreto, L. S. Influence of hydrothermal carbonization on formation of curved graphite structures obtained from a lignocellulosic precursor. *Carbon* **2014,** 78, 609-612. doi: https://doi.org/10.1016/j.carbon.2014.07.017

(18) Demir, M.; Kahveci, Z.; Aksoy, B.; Palapati, N. K. R.; Subramanian, A.; Cullinan, H. T.; El-Kaderi, H. M.; Harris, C. T.; Gupta, R. B. Graphitic biocarbon from metal-catalyzed hydrothermal carbonization of lignin. *Ind. Eng. Chem. Res.* **2015,** 54, 10731-10739. doi: https://doi.org/10.1021/acs.iecr.5b02614

(19) Legarra, M.; Morgan, T.; Turn, S.; Wang, L.; Skreiberg, Ø.; Antal, M. J. Carbonization of biomass in constant-volume reactors. *Energy & Fuels* **2018,** 32, 475-489. doi: https://doi.org/10.1021/acs.energyfuels.7b02982

(20) Wang, L.; Skreiberg, Ø.; Gronli, M.; Specht, G. P.; Antal, M. J. Is elevated pressure required to achieve a high fixed-carbon yield of charcoal from biomass? Part 2: The importance of particle size. *Energy & Fuels* **2013,** 27, 2146-2156. doi: https://doi.org/10.1021/ef400041h

(21) Van Wesenbeeck, S.; Higashi, C.; Legarra, M.; Wang, L.; Antal, M. J. Biomass pyrolysis in sealed vessels. Fixed-carbon yields from avicel cellulose that realize the theoretical limit. *Energy & Fuels* **2016,** 30, 480-491. doi: https://doi.org/10.1021/acs.energyfuels.5b02628

(22) Legarra, M.; Morgan, T.; Turn, S.; Wang, L.; Skreiberg, Ø.; Antal, M. J. Effect of processing conditions on the constant-volume carbonization of biomass. *Energy & Fuels* **2019,** 33, 2219-2235. doi: https://doi.org/10.1021/acs.energyfuels.8b03433

(23) Wang, Y.; Alsmeyer, D. C.; McCreery, R. L. Raman spectroscopy of carbon materials: Structural basis of observed spectra. *Chem. of Mater.* **1990,** 2, 557-563. doi: https://doi.org/10.1021/cm00011a018

(24) Vázquez-Santos, M. B.; Geissler, E.; László, K.; Rouzaud, J.-N.; Martínez-Alonso, A.; Tascón, J. M. D. Comparative XRD, raman, and TEM study on graphitization of PBO-derived carbon fibers. *J. Phys. Chem. C.* **2012,** 116, 257-268. doi: https://doi.org/10.1021/jp2084499

(25) Chen, K.; Zhang, H.; Ibrahim, U.-K.; Xue, W.; Liu, H.; Guo, A. The quantitative assessment of coke morphology based on the raman spectroscopic characterization of serial petroleum cokes. *Fuel* **2019,** 246, 60-68. doi: https://doi.org/10.1016/j.fuel.2019.02.096

(26) Potgieter-Vermaak, S.; Maledi, N.; Wagner, N.; Van Heerden, J. H. P.; Van Grieken, R.; Potgieter, J. H. Raman spectroscopy for the analysis of coal: A review. *J. Raman Spect.* **2011,** 42, 123-129. doi: https://doi.org/10.1002/jrs.2636

(27) Hiestand, E. N. Tablet bond. I. A theoretical model. *Int. J. Pharm.* **1991,** 67, 217-229. doi: https://doi.org/10.1016/0378-5173(91)90205-3

(28) Williams, O. A.-O.; Taylor, S.; Lester, E.; Kingman, S.; Giddings, D.; Eastwick, C. Applicability of mechanical tests for biomass pellet characterisation for bioenergy applications. *Materials* **2018,** 11, 1329-1347. doi: https://doi.org/10.3390/ma11081329

(29) Sun, C. C. Decoding powder tabletability: Roles of particle adhesion and plasticity. *J. Adhesion Sci. & Tech.* **2011,** 25, 483-499. doi: https://doi.org/10.1163/016942410X525678

(30) Nguyen, H. G. T.; Horn, J. C.; Bleakney, M.; Siderius, D. W.; Espinal, L. Understanding material characteristics through signature traits from helium pycnometry. *Langmuir* **2019,** 35, 2115-2122. doi: https://doi.org/10.1021/acs.langmuir.8b03731

(31) Mao, J. D.; Johnson, R. L.; Lehmann, J.; Olk, D. C.; Neves, E. G.; Thompson, M. L.; Schmidt-Rohr, K. Abundant and stable char residues in soils: Implications for soil fertility and carbon sequestration. *Environ. Sci. Technol.* **2012,** 46, 9571-9576. doi: https://doi.org/10.1021/es301107c

(32) Johnson, R. L.; Schmidt-Rohr, K. Quantitative solid-state ^{13}C nmr with signal enhancement by multiple cross polarization. *J. Mag. Reson.* **2014,** 239, 44-49. doi: https://doi.org/10.1016/j.jmr.2013.11.009

(33) Lawrinenko, M.; Laird, D. A.; Johnson, R. L.; Jing, D. Accelerated aging of biochars: Impact on anion exchange capacity. *Carbon* **2016,** 103, 217-227. doi: https://doi.org/10.1016/j.carbon.2016.02.096

(34) Johnson, R. L.; Anderson, J. M.; Shanks, B. H.; Schmidt-Rohr, K. Simple one-step synthesis of aromatic-rich materials with high concentrations of hydrothermally stable catalytic sites, validated by NMR. *Chem. Mater.* **2014,** 26, 5523-5532. doi: https://doi.org/10.1021/cm501562t

(35) Couderc, P.; Hyvernat, P.; Lemarchand, J. L. Correlations between ability of pitch to penetrate coke and the physical characteristics of prebaked anodes for the aluminium industry. *Fuel* **1986,** 65, 281-287. doi: https://doi.org/10.1016/0016-2361(86)90022-0

(36) Plancher, H.; Agarwal, P.; Severns, R. Improving form coke briquette strength. *Fuel Processing Tech.* **2002,** 79, 83-92. doi: https://doi.org/10.1016/S0378-3820(02)00105-4

Author Accepted Manuscript version of the paper by Robert Johnson et al.
in ACS Sustainable Chemistry & Engineering Vol. 11 (2023) Page, DOI: http://dx.doi.org/10.1021/acssuschemeng.2c05229

673 **TOC Abstract Graphic**

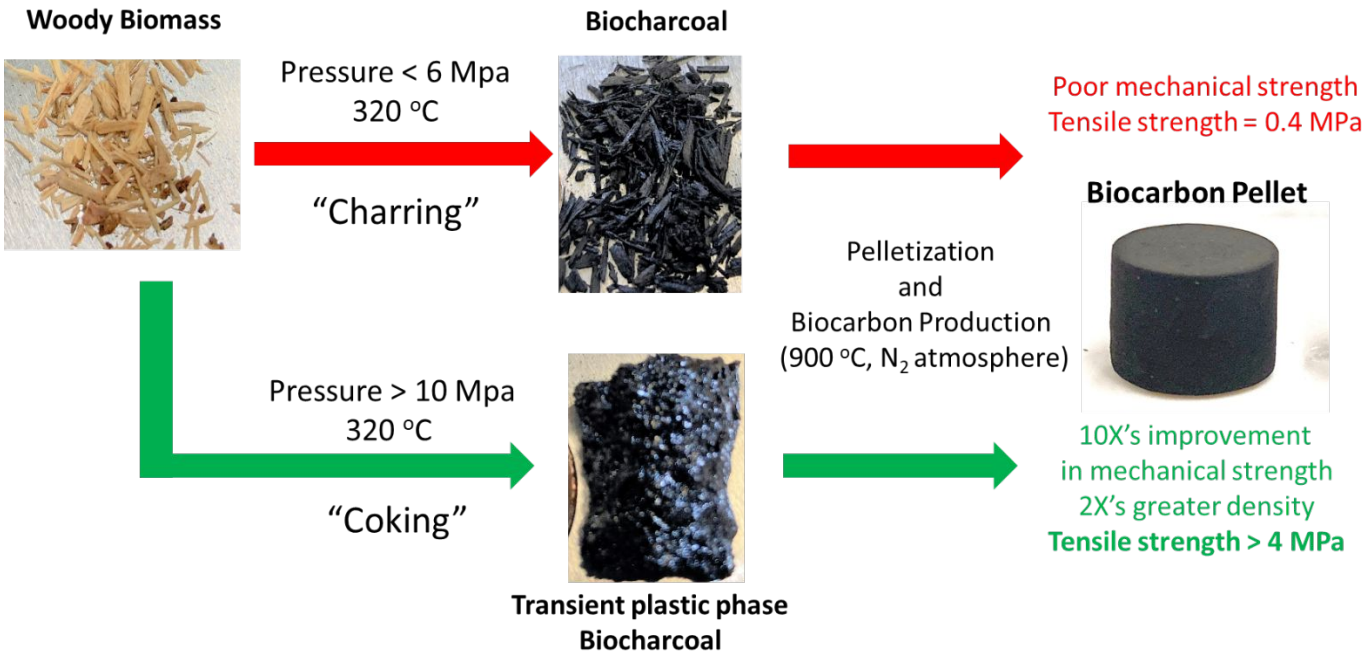

674

675 **Synopsis:**

676 Pressurized pyrolysis of birch stem wood produced transient plastic phase biochar whose pellets displayed

677 enhanced tensile strength (>4 MPa).